Repetitive emissions of rising-tone chorus waves in the inner magnetosphere

Quanming Lu (qmlu@ustc.edu.cn)
University of Science and Technology of China https://orcid.org/0000-0003-3041-2682
Xueyi Wang
Auburn University
Lunjin Chen
University of California Los Angeles
Xinliang Gao
University of Science and Technology of China
Yu Lin
Auburn University
S. Wang
University of Science and Technology of China

Article

Keywords: Chorus Emissions, Azimuthal Drift, Discrete and Continuous Spectra

Posted Date: September 29th, 2020

DOI: https://doi.org/10.21203/rs.3.rs-75226/v1

Version of Record: A version of this preprint was published at Geophysical Research Letters on August 1st, 2021. See the published version at https://doi.org/10.1029/2021GL094979.

Repetitive emissions of rising-tone chorus waves in the inner magnetosphere

Quanming Lu[1,2,5*], Xueyi Wang[3,5*], Lunjin Chen[4,5*], Xinliang Gao[1,2], Yu Lin[3], and Shui Wang[1,2]

[1]CAS Key Laboratory of Geospace Environment, Department of Geophysics and Planetary Science, University of Science and Technology of China, Hefei 230026, China

[2]CAS Center for Excellence in Comparative Planetology, China

[3]Physics Department, Auburn University, Auburn, Alabama, USA

[4]Department of Physics, University of Texas at Dallas, Richardson, Texas, USA

[5]These authors contributed equally: Quanming Lu, Xueyi Wang, Lunjin Chen

Email: qmlu@ustc.edu.cn; xywang@physics.auburn.edu;lunjin.chen@gmail.com

Abstract

Chorus waves are well known for their significant roles in the radiation belts of the Earth and other magnetized planets, including acceleration of electrons to relativistic energies, and precipitation of energetic electrons into the ionosphere to produce diffuse and pulsating aurora. They typically occur in the form of discrete and repetitive quasi-monochromatic emissions with a frequency chirping, which was discovered more than 50 years ago. However, until now there is still no satisfactory explanations for repetitive emissions of chorus waves. In this report, chorus emissions excited by energetic electrons with a temperature anisotropy are studied by both a one-dimensional δf simulation and theoretical model in a dipole magnetic field. The two models have unanimously demonstrated that a continuous injection of energetic electrons caused by an azimuthal drift is essential for the repetitive emissions of chorus waves. Consistent with satellite observations, both discrete and continuous spectra can be reproduced. An intense injection of energetic electrons will lead to a decrease of the time separation between the chorus elements, and the chorus emissions evolve from a discrete to a continuous spectrum when the injection is sufficiently strong.

Introduction

Chorus waves are electromagnetic emissions that are commonly observed in geospace consisting of ionized gas (plasma) embedded with a magnetic field, and known for an ensemble of distinct elements with each showing frequency chirping[1-5]. Such frequency chirping in every element is often featured with a rising frequency (over ~1 kHz) over a short duration of period (~ 0.1 seconds). Chorus waves are so named to reflect similar frequency-time variation to birds' dawn chorus in acoustic mode. Such electromagnetic chorus waves have well-known for their significant roles in geospace phenomena, to name a few, acceleration of electrons to relativistic energy and thus the formation of Earth's radiation belts[6-9]; precipitation of electrons into the ionosphere, and thus generation of diffuse and pulsating aurora[10-14]. The exhibition of a series of short-living microburst often seen in electron precipitation is generally considered to be caused by the repetitive emissions of chorus elements[15-17].

Rising-tone chorus waves have been successfully reproduced in particle-in-cell (PIC) simulations, and their formation is considered to be fulfilled through nonlinear wave-particle interaction[18-23]. An electromagnetic electron hole in the wave phase space is formed after resonant electrons have been trapped by whistler-mode waves, and then a resonant current is generated when the background magnetic field has a spatial inhomogeneity, which at last results in rising-tone chorus waves[19,20,24]. However, these PIC simulations were performed in an isolated system, where electrons are forced to be bounded along a single field line. Such an isolated system is not realistic in that electrons are subject to azimuthal drift across the field line where chorus elements are excited. For these simulations, only one distinct element of rising-tone chorus has been observed since the free energy stored in the electron distribution is released in a burst way, and the repetitive feature as typically shown in satellite observations cannot be reproduced[22]. In this report, with both a one-dimensional (1-D) δf PIC simulation and theoretical models, where a continuous injection of energetic electrons with a

temperature anisotropy caused by the azimuthal drift is implemented, we demonstrate the generation mechanism of repetitive emissions of rising-tone chorus waves.

Results

Measurements of repetitive chorus emissions. Chorus waves in the radiation belt typically exhibit discrete and repetitive emissions with a rising frequency. Fig. 1 shows the spectrogram of magnetic power for three typical types of chorus waves observed by the Van Allen Probes. In Fig 1a, only one element is observed. There is an ensemble of discrete and repetitive elements in Fig. 1b, and the average time separation between the elements is about 0.2s. In Fig. 1c the time separation between the elements is very small (compared with the duration of individual elements), and the spectrogram looks like a continuous spectrum. The frequencies of these waves range from ~0.2f_{ce} to ~0.45f_{ce}. In general, the second and third types of chorus waves are ubiquitously observed in the radiation, while the first type can also be identified from time to time.

δf simulations of repetitive chorus emissions: A one-dimensional (1-D) δf simulation model is developed to study the emissions of rising-tone chorus waves in a dipole magnetic field. In this model, energetic electrons with a temperature anisotropy are injected continuously into the simulation domain due to the azimuthal drift. The details of the model and simulation setup can be found in the supplementary information.

Fig. 2 plots the spectrogram of wave magnetic power at the latitude $\lambda = 15^0$, which is obtained from the 1-D δf simulations. For the case of $\Omega_{e0}\tau_D = \infty$, where energetic electron injection into the system is turned off, only one rising-tone element forms(Fig. 2a). This case is similar to that of an isolated system, which has been studied by many previous particle-in-cell (PIC) simulations[21-23]. In such a situation, the free energy is provided by the initial anisotropic distribution of energetic electrons, and in general only one element of chorus waves is generated. When energetic electrons are injected continuously into the system, the chorus waves exhibit repetitive elements with a rising frequency. With the intensification of the energetic electron injection (through

the decrease of $\Omega_{e0}\tau_D$), the time separation between the elements become smaller and smaller. At $\Omega_{e0}\tau_D = 2000$, the chorus waves display an ensemble of discrete and repetitive elements as shown in Fig. 2b. The average time separation between the elements is about $1000\,\Omega_{e0}^{-1}$. If we use the magnetic field at L=5, the time separation is estimated to be around 0.05s. When the injection of energetic electrons is sufficiently intense, the time separation between the elements is even smaller and spectrogram looks like an almost continuous spectrum. The frequencies of these waves range from ~0.2 Ω_{e0} to ~$0.75\,\Omega_{e0}$.

Obviously, the spectrogram obtained in our 1-D δf simulations is similar to that of the satellite observations shown in Fig. 1. Our simulations found that the injection of energetic electrons, which can resonantly interact with the chorus waves, plays an important role to mediate the repetitive emissions of chorus waves in the radiation belt. The injection is considered to be caused by the azimuthal drift in the dipole magnetic field. According to the measured plasma and wave parameters by the Van Allen Probes, the parallel energy of electrons resonantly interacting with the chorus waves, calculated as $E_{\parallel} = 1/2 m_e V_R^2$ (where V_R is the parallel velocity of the resonant electrons) is about 13.1, 69.1 and 79.8keV, corresponding to those in Fig. 1a-c. Then, for electron equatorial pitch angle of 45°, their azimuthal drift velocities due to magnetic curvature and gradient are estimated to be 0.0077, 0.021, $0.033\,V_A$ (where V_A is the Alfven speed defined by the local magnetic field and plasma density), respectively. Therefore, we can find that with the increase of the azimuthal drift velocity of the resonant electrons, the chorus emissions change from a single element (Fig. 1a) to an ensemble of discrete and repetitive elements (Fig. 1b), and to an almost continuous spectrum (Fig. 1c). Because the increase of the azimuthal drift will lead to the decrease of τ_D (or equivalently more intense injection of energetic electrons), our simulations are consistent with the satellite observations shown in Fig. 1. Please also note, in the simulations we used a reduced magnetic topology in order to save computational source,

and nowadays it remains computationally challenging to compare the simulations with the observations quantitatively.

It is generally accepted that chorus waves are excited as a result of electron holes in the wave-particle interaction angle (ζ), which are formed by electrons resonantly trapped in the waves. Similarly, we can also find such kind of electron holes in our δf simulations. A typical electron hole at $\Omega_{e0}t = 6700$ for the case with $\Omega_{e0}\tau_D$ =2000 is shown in Fig. 3a by plotting the electron distributions $\delta f(v_{\|},\zeta)$ at different values of $v_{\perp}/V_{\|te}$ (where ζ is the angle made by electron perpendicular velocity and wave perpendicular magnetic field vector, and $V_{\|te}$ is the thermal velocity of energetic electrons). The hole only exists in the range $v_{\perp}/V_{\|te}$ from ~0.5 to ~6.5 (Fig. 3a). By comparing Fig. 2a and Fig. 3b-d, we can find that each chorus element is accompanied by an electron hole and their duration in time are comparable.

Theoretical model of repetitive chorus emissions: In order to better understand the repetitive emissions of chorus waves in a dipole magnetic field, we further propose a modification on the theoretical model developed by Omura et al.[19] to account for the effect of electron injection. The temporal variation for the amplitude and frequency of chorus waves near the equator is governed by the followed equations

$$\frac{\partial \tilde{B}_w}{\partial \tilde{t}} = c_1 G \tilde{B}_w^{1/2} - c_2 \tilde{\omega}^{-1}, \quad (1)$$

$$\frac{\partial \tilde{\omega}}{\partial \tilde{t}} = c_3 \tilde{\omega} \tilde{B}_w. \quad (2)$$

where $\tilde{B}_w = B_w / B_0$ (B_w is the amplitude of chorus waves, and B_0 is the amplitude of the background magnetic field at the equator), $\tilde{\omega} = \omega/\Omega_{e0}$ ($\Omega_{e0} = eB_0/m_e$), and $\tilde{t} = \Omega_{e0}t$. The first term at the right of Eq. (1) corresponds to the nonlinear growth of the chorus waves, and the second term describes the damping caused due to the inhomogeneity along the magnetic field line. To account for the effects of electron

injection and the wave scattering to the electron distribution, we introduced a factor $G(t)$, which denotes the resonant electron distribution normalized to that at initial time. In the theory by Omura et al.[19], the electron distribution is assumed to be unchanged, corresponding to the case when G is a constant of 1. The definition of c1, c2 and c3, which are functions of $\tilde{\omega}$, can be obtained by comparing Eqs. (1-2) with Eqs. (40-41) in Omura et al.[19].

We propose the following equation to describe the introduced resonant distribution function G

$$\frac{\partial G}{\partial \tilde{t}} = -c_4 G \tilde{B}_w^2 + \frac{G_0 - G}{\tilde{\tau}_D}. \quad (3)$$

The first term at the right side of Eq. (3) describes the reduction of resonant electrons caused by the scattering of chorus waves, which is proportional to wave power $\tilde{B}_w^2$, and the second term corresponds to the injection of energetic electrons, which leads to recover the resonant electrons' initial distribution G_0 (=1) with the time scale $\tilde{\tau}_D$ controlling the rate of electron injection. Since the chorus waves are often terminated at half electron gyrofrequency, we only limit the calculation for $\tilde{\omega}$ up to $1/2$.

From Eq. (1)-(3), we can calculate the time evolution of the amplitude $\tilde{B}_w$ and frequency of chorus waves $\tilde{\omega}$, as well as the normalized resonant distribution function G. For illustration purpose, we set a typical value for $c_1 = 2\text{x}10^{-4}$, $c_2 = 1.5\text{x}10^{-7}$, $c_3 =$ =0.5, $c_4 = 5\text{x}10^2$, with their dependence on wave frequency ignored. Following Omura et al.[19], the initial condition is set as $\tilde{\omega}$=0.2 and $\tilde{B}_w = 2.5\text{x}10^{-4}$. The results for $\tilde{\tau}_D = \infty$, 2000, and 400 are shown in Fig. 4. Consistent with δf simulations, we can find that for $\tilde{\tau}_D = \infty$ (no injection) there is only one element of chorus waves. The repetitive emissions of rising-tone chorus waves are observed when there is an injection of energetic electrons, and the time separation between the chorus elements decrease with

the intensification of the injection (decreasing $\tilde{\tau}_D$). The general characteristics of the variation of the three variables are as follows. When G is sufficient large, a nonlinear wave growth leads to an increasing amplitude (Eq. (1)). Accompanied with it, the frequency increases (Eq. (2)) and thus a chorus element is formed. During the chorus element formation, the free energy is released and thus G is reduced rapidly due to the wave scattering term (Eq. (3)). As the chorus element is terminated, so does the wave scattering. The refilling due to electron injection starts to replenish the electron distribution by recovering G to the initial value. When G exceeds the threshold imposed by Eq. (1), another cycle of chorus electron formation starts. How fast G exceeds the threshold depends on the refilling rate $\tilde{\tau}_D$, which explains the dependence of the time separation of chorus elements on $\tilde{\tau}_D$.

Conclusions and Discussion

In this report, we at first developed a 1-D δf simulation model to study chorus emissions in a dipole magnetic field, where the injection of anisotropic energetic electrons is implemented. The injection of energetic electrons through the azimuthal drift into the field line of chorus excitation is found to play a critical role to generate the repetitive emissions of rising-tone chorus waves. When the injection is considered, the chorus waves exhibit an ensemble of discrete and repetitive elements, and each element is accompanied by an electromagnetic electron holes in the wave-particle interaction phase space. The time separation between the elements shortens with the intensification of the injection, which is consistent with satellite observations. The repetitive emissions of chorus waves are then also reproduced by a proposed theoretical model.

Discrete and repetitive emissions of chorus waves are ubiquitously observed in the earth's radiation belt, and both our theoretical and δf simulation models show that such kind of repetitive emissions is mediated by the injection of energetic electrons caused by the azimuthal drift in the dipole field. Chorus waves are also observed as a

194 hiss-like emission with an apparently continuous spectrum, and do not have discrete
195 elements[25]. Such continuous spectrum can also be accounted for by the effect of
196 electron injection. When the injection is sufficiently strong, the time separation between
197 elements becomes small in comparison with individual element duration. As a result,
198 the elements will overlap each other and chorus waves of a continuous spectrum form.

199 ## Method

200 **1-D δf PIC simulation model with an injection of energetic electrons:** One-
201 dimensional (1-D) δf particle-in-cell (PIC) simulations are performed in this report to
202 study chorus emissions in a dipole magnetic field. In the simulations, there are two
203 electron components: cold and energetic electrons. Both of them are considered as
204 particles, and are subject to the Lorentz force. Ions are motionless. A continuous
205 injection of energetic electrons caused by an azimuthal drift in a dipole magnetic field
206 is considered in the model as schematically shown by Fig. 5. Due to the azimuthal drift,
207 energetic electrons with a distribution f_0 are injected into the simulation domain, and
208 energetic electrons leaving the simulation domain have a distribution f. Therefore,
209 the evolution of the electron distribution is governed by the following modified Vlasov
210 equation:

211 $$\frac{\partial f}{\partial t}+\dot{\xi}\frac{\partial f}{\partial \xi}+\dot{\mathbf{u}}\cdot\frac{\partial f}{\partial \mathbf{u}}=-\frac{f-f_0}{\tau_D} \tag{4}$$

212 where ξ is the coordinate along the magnetic field line, $\mathbf{u}=\gamma\mathbf{v}$ ($\mathbf{v}$ is the particle
213 velocity, and γ is the Lorentz factor). τ_D is a time scale related to the injection of
214 energetic electrons caused due to the azimuthal drift.

215 We split the electron distribution into a background and perturbed parts,
216 $f=f_0+\delta f$, and the evolution of δf is determined by

$$\frac{\partial \delta f}{\partial t}+\dot{\xi}\frac{\partial \delta f}{\partial \xi}+\dot{\mathbf{u}}\cdot\frac{\partial \delta f}{\partial \mathbf{u}}=-\dot{\mathbf{u}}_1\cdot\frac{\partial f_0}{\partial \mathbf{u}}-\frac{\delta f}{\tau_D} \tag{5}$$

where $\dot{\mathbf{u}}_1=e(\delta\mathbf{E}+\mathbf{v}\times\delta\mathbf{B})/m_e$ (e and m_e are the electron charge and mass). $\delta\mathbf{E}=\mathbf{E}-\mathbf{E}_0$ and $\delta\mathbf{B}=\mathbf{B}-\mathbf{B}_0$ are the perturbed electromagnetic field, where $\mathbf{E}_0$ and $\mathbf{B_0}$ are the equilibrium electromagnetic field.

The equation for the evolution of perturbed particle weighting function, $w=\delta f/f=(f-f_0)/f$, is thus obtained.

$$\frac{dw}{dt}=-\frac{w}{\tau_D}+\frac{w^2}{\tau_D}+(1-w)\dot{\mathbf{u}}_1\cdot\frac{\partial \ln f_0}{\partial \mathbf{u}} \tag{6}$$

In the δf scheme, the perturbed electromagnetic field are advanced from Maxwell equations:

$$\begin{aligned}
&\nabla\times\delta\mathbf{E}=-\frac{\partial\delta\mathbf{B}}{\partial t}\\
&\nabla\times\delta\mathbf{B}=\mu_0\delta\mathbf{J}+\frac{1}{c^2}\frac{\partial\delta\mathbf{E}}{\partial t}\\
&\nabla\cdot\delta\mathbf{E}=\frac{\delta\rho}{\varepsilon_0}\\
&\nabla\cdot\delta\mathbf{B}=0
\end{aligned} \tag{7}$$

where the perturbed current is $\delta\mathbf{J}=-e\int\mathbf{v}\delta f dv^3$, and the perturbed charge density is $\delta\rho=-e\int\delta f dv^3$.

Initially, the distribution of energetic electrons is assumed to satisfy the bi-Maxwellian function at the equator as follows. the ratio of the number density of energetic electrons to that of cold electrons is $n_{h0}/n_{c0}=0.6\%$, the ratio of cold electron plasma frequency to electron gyrofrequency is $\omega_{pe}/\Omega_{e0}=4.97$ （ where $\omega_{pe}=\sqrt{n_0e^2/m_e\varepsilon_0}$ is the electron plasma frequency, $n_0=n_{c0}+n_{h0}$, and $\Omega_{e0}=eB_{0eq}/m_e$ is the electron gyrofrequency at the equator ）, the temperature

anisotropy of energetic electrons is $T_{\perp 0}/T_{\|0}$=6, and the parallel plasma beta of energetic electrons is $\beta_{\|h0} = n_{h0}T_{\|0}/(B_{0eq}^2/2\mu_0) = 0.01$. These parameters are typical values at L=5, and the other values of these parameters off the equator along the magnetic field can be obtained with the Liouville's theorem[23]. In the simulations, there are 4000 grid number, and grid cell is $0.34d_e$ (where $d_e = c/\omega_{pe}$ is the electron inertial length). The topology of the magnetic field in the simulations is roughly equal to that at L=0.6, and the latitude ranges from about -32^0 to 32^0. On average, there are about 4000 particles per cell, and the time step is $0.03\,\Omega_{e0}^{-1}$. Absorbing boundary condition is applied for the electromagnetic field, while reflecting boundary is applied for particles.

Data availability

The entire Van Allen Probes dataset is publicly available at https://spdf.gsfc.nasa.gov/pub/data/rbsp/.

Code availability

The computer code of δf simulation in this work is available upon request to the corresponding author.

References

1. Burtis, W. J., and R. A. Helliwell (1969), Banded chorus—A new type of VLF radiation observed in the magnetosphere by OGO 1 and OGO 3, J. Geophys. Res., 74(11), 3002–3010, doi:10.1029/JA074i011p03002.
2. Tsurutani, B. T., and E. J. Smith (1974), Postmidnight chorus: A substorm phenomenon, J. Geophys. Res., 79(1), 118–127, doi:10.1029/JA079i001p00118.
3. Tsurutani, B. T., and E. J. Smith (1977), Two types of magnetospheric ELF chorus

and their substorm dependences, J. Geophys. Res., 82(32), 5112–5128, doi:10.1029/JA082i032p05112.

4. Meredith, N. P., R. B. Horne, and R. R. Anderson (2001), Substorm dependence of chorus amplitudes: Implications for the acceleration of electrons to relativistic energies, J. Geophys. Res., 106(A7), 13,165–13,178, doi:10.1029/2000JA900156.

5. Li, W., R. M. Thorne, J. Bortnik, X. Tao, and V. Angelopoulos (2012), Characteristics of hiss-like and discrete whistler mode emissions, Geophys. Res. Lett., 39, L18106, doi:10.1029/2012GL053206.

6. Summers, D., R. M. Thorne, and F. L. Xiao (1998), Relativistic theory of wave-particle resonant diffusion with application to electron acceleration in the magnetosphere, J. Geophys. Res., 103(A9), 20,487–20,500, doi:10.1029/98JA01740.

7. Horne, R. B., R.M. Thorne, S. A. Glauert, J. M. Albert, N. P.Meredith, and R. R. Anderson (2005), Timescale for radiation belt electron acceleration by whistler mode chorus waves, J. Geophys. Res., 110, A03225, doi:10.1029/2004JA010811.

8. Xiao, F. L., Z. P. Su, H. N. Zheng, and S. Wang(2009), Modeling of outer radiation belt electron by multidimensional diffusion process, J. Geophys. Res., 114, A03201, doi:10.1029/2008JA013580

9. Thorne, R. M., et al. (2013), Rapid local acceleration of relativistic radiation-belt electrons by magnetospheric chorus, Nature, 504(7480), 411, doi:10.1038/Nature12889.

10. Lorentzen, K. R., J. B. Blake, U. S. Inan, and J. Bortnik (2001), Observations of relativistic electron microbursts in association with VLF chorus, J. Geophys. Res., 106(A4), 6017–6027, doi:10.1029/2000JA003018.

11. Thorne, R. M., T. P. O'Brien, Y. Y. Shprits, D. Summers, and R. B. Horne (2005), Timescale for MeV electron microburst loss during geomagnetic storms, J. Geophys. Res., 110, A09202, doi:10.1029/2004JA010882.

12. Ni, B., R. M. Thorne, Y. Y. Shprits, and J. Bortnik(2008), Resonant scattering of plasma sheet electrons by whistler-mode chorus: Contribution to diffuse auroral precipitation, Geophys. Res. Lett., 35, L11106, doi:10.1029/2008GL034032.

291 13. Thorne, R. M., B. Ni, X. Tao, R. B. Horne, and N. P. Meredith (2010), Scattering
292 by chorus wave as the dominant cause of diffuse auroral precipitation, Nature, 467,
293 934-936, doi:10.1038/nature09467.
294 14. Lam, M. M., R. B. Horne, N. P. Meredith, S. A. Glauert, T. Moffat-Griffin, and J.
295 C. Green (2010), Origin of energetic electron precipitation >30 keV into the
296 atmosphere, J. Geophys. Res., 115, A00F08, doi:10.1029/2009JA014619.
297 15. Hikishima, M., Y. Omura, and D. Summers (2010), Microburst precipitation of
298 energetic electrons associated with chorus wave generation, Geophys. Res. Lett.,
299 37, L07103, doi:10.1029/2010GL042678
300 16. Mozer, F. S., O. V. Agapitov, J. B. Blake, and I. Y. Vasko (2018), Simultaneous
301 observations of lower band chorus emissions at the equator and microburst
302 precipitating electrons in the ionosphere, Geophys. Res. Lett., 45, 511-516,
303 doi:10.1002/2017GL076120
304 17. Tsurutani, B. T., G. S. Lakhina, and O. P. Verkhoglyadova (2013), Energetic
305 electron (>10 keV) microburst precipitation, _5–15 s X-ray pulsations, chorus,
306 and wave-particle interactions: A review, J. Geophys. Res. Space Physics, 118,
307 doi:10.1002/jgra.50264.
308 18. Katoh, Y., and Y. Omura (2006), A study of generation mechanism of VLF triggered
309 emission by self-consistent particle code, J. Geophys. Res., 111, A12207,
310 doi:10.1029/2006JA011704.
311 19. Omura, Y., Y. Katoh, and D. Summers (2008), Theory and simulation of the
312 generation of whistler-mode chorus, J. Geophys. Res., 113, A04223,
313 doi:10.1029/2007JA012622.
314 20. Hikishima, M., and Y. Omura (2012), Particle simulations of whistler-mode rising-
315 tone emissions triggered by waves with different amplitudes, J. Geophys. Res.,
316 117, A04226, doi:10.1029/2011JA017428.
317 21. Tao, X. (2014), A numerical study of chorus generation and the related variation of
318 wave intensity using the DAWN code, J. Geophys. Res. Space Physics, 119,
319 3362–3372, doi:10.1002/2014JA019820.
320 22. Ke Y., X. Gao, Q. Lu, X. Wang, and S. Wang (2017), Generation of risingtone

chorus in a two-dimensional mirror field by using the general curvilinear PIC code, J. Geophys. Res. Space Physics, 122, 8154–8165, doi:10.1002/2017JA024178.

23. Lu, Q., Ke, Y., Wang, X., Liu, K., Gao, X., Chen, L., & Wang, S. (2019). Two-dimensional general curvilinear particle-in-cell (gcPIC) simulation of rising-tone chorus waves in a dipole magnetic field. Journal of Geophysical Research: Space Physics, 124, 4157–4167. https://doi.org/10.1029/2019JA026586

24. Omura, Y., and D. Summers (2006), Dynamics of high-energy electrons interacting with whistler mode chorus emissions in the magnetosphere, J. Geophys. Res., 111, A09222, doi:10.1029/2006JA011600

25. Gao, X. L., W. Li, R. M. Thorne, J. Bortnik, V. Angelopoulos, Q. M. Lu, X. Tao, and S. Wang (2014), New evidence for generation mechanisms of discrete and hiss-like whistler mode waves, Geophys. Res. Lett., 41, 4905-4811.

Acknowledgements:

This work was supported by the NSFC grant 41774169, and Key Research Program of Frontier Sciences, CAS(QYZDJ-SSW-DQC010).

Author contributions

Q. L. supervised the work and coordinated the results from spacecraft observation, numerical simulations and theory; X. W. performed simulations; L. C. proposed the theoretical model; Q. L., X. W, and L. C. contributed to writing the manuscript. X. G. carried out spacecraft data analysis; Y. L. and S. W. participated in this research by analyzing and interpreting theoretical and observational results.

Competing interests

The authors declare no competing interests.

Figures

Figure 1 The spectrogram of magnetic power for three examples of chorus waves observed by the Van Allen Probes. All the chorus waves were detected by the Electric Magnetic Field Instrument Suite and Integrated Science (EMFISIS) on Van Allen Probe A. **a** The waves detected from 2014-04-30/19:33:29, in L-shell value=5.38, magnetic local time (MLT)=9.1hr, and magnetic latitude (MLAT)=-0.7°. There is only one discrete element. The background magnetic field is about 153.0nT, and the plasma density is about 9.1cm^{-3}. The wave normal angle of the chorus waves is about 22.1^0, and the lowest frequency is about 1000Hz~0.23f_{ce}. **b** The wave detected from 2013-03-01/14:29:28.0, in L=5.06, MLT=2.7hr, and MLAT=-0.9°. There is an ensemble of discrete and repetitive elements. The background magnetic field is about 144.6nT, and the plasma density is about 2.0cm^{-3}. The wave normal angle of the chorus waves is about 11.1^0, and the lowest frequency is about 800Hz~0.20f_{ce}. **c** The waves detected from 2013-03-01/14:09:21.0, in L=5.31, MLT=2.4hr, and MLAT=-1.5°. The spectrogram looks like a continuous spectrum. The background magnetic field is about 124.7nT, and the plasma density is about 2.3cm^{-3}. The wave normal angle of the chorus waves is about 21.4^0, and the lowest frequency is about 500Hz~0.14f_{ce}. In the figure, the dotted and dashed lines in black or white represent 0.1f_{ce} and 0.5f_{ce}, respectively. Here f_{ce} is the electron gyrofrequency at the equator.

Figure 2 The spectrogram of magnetic power for chorus waves obtained at the latitude λ= 15^0 from the δf simulations. **a** $\Omega_{e0}\tau_D = \infty$. **b** $\Omega_{e0}\tau_D = 2000$. **c** $\Omega_{e0}\tau_D = 400$. Here, the dotted and dashed lines in black or white represent $0.1\,\Omega_{e0}$ and $0.5\,\Omega_{e0}$, respectively, and $\Omega_{e0}(=2\pi f_{ce})$ is the electron gyrofrequency at the equator. The frequencies of these waves range from ~$0.2\,\Omega_{e0}$ to ~$0.75\,\Omega_{e0}$.

Figure 3 Electron holes associated with chorus waves obtained at the latitude λ= 15^0 from the δf simulations. a Electron distributions $\delta f(v_{\parallel},\zeta)$ at different

values of $v_\perp / V_{\|te}$ for the selected hole at $\Omega_{e0}t = 6700$ for the case with $\Omega_{e0}\tau_D$ =2000. **b-d** The time evolution of electron distributions $\delta f(v_\|)$ at ζ=0.8π and $v_\perp / V_{\|te}$ =2.25 for the three cases, $\Omega_{e0}\tau_D = \infty$, 2000, and 400, respectively.

Figure 4 The time evolution for the amplitude ($\tilde{B}_w$) and frequency ($\tilde{\omega}$) of chorus waves, as well as the resonant distribution function (G). a $\Omega_{e0}\tau_D = \infty$. **b** $\Omega_{e0}\tau_D = 2000$. **c** $\Omega_{e0}\tau_D = 400$. The calculation is based on Eq. (1)-(3). The blue, red and black lines represent the amplitude **(** $\tilde{B}_w$ **)** , frequency **(** $\tilde{\omega}$ **)** and resonant distribution function (G), respectively.

Figure 5 The schmetic diagram for the evolution of energetic electrons in a dipole magnetic field. Due to an azimuthal drift, energetic electrons with a distribution f_0 is injected into the simulation domain, while particles leaving the domain have a distribution f . The blue-shaded region is the region of chorus wave excitation.

Figures

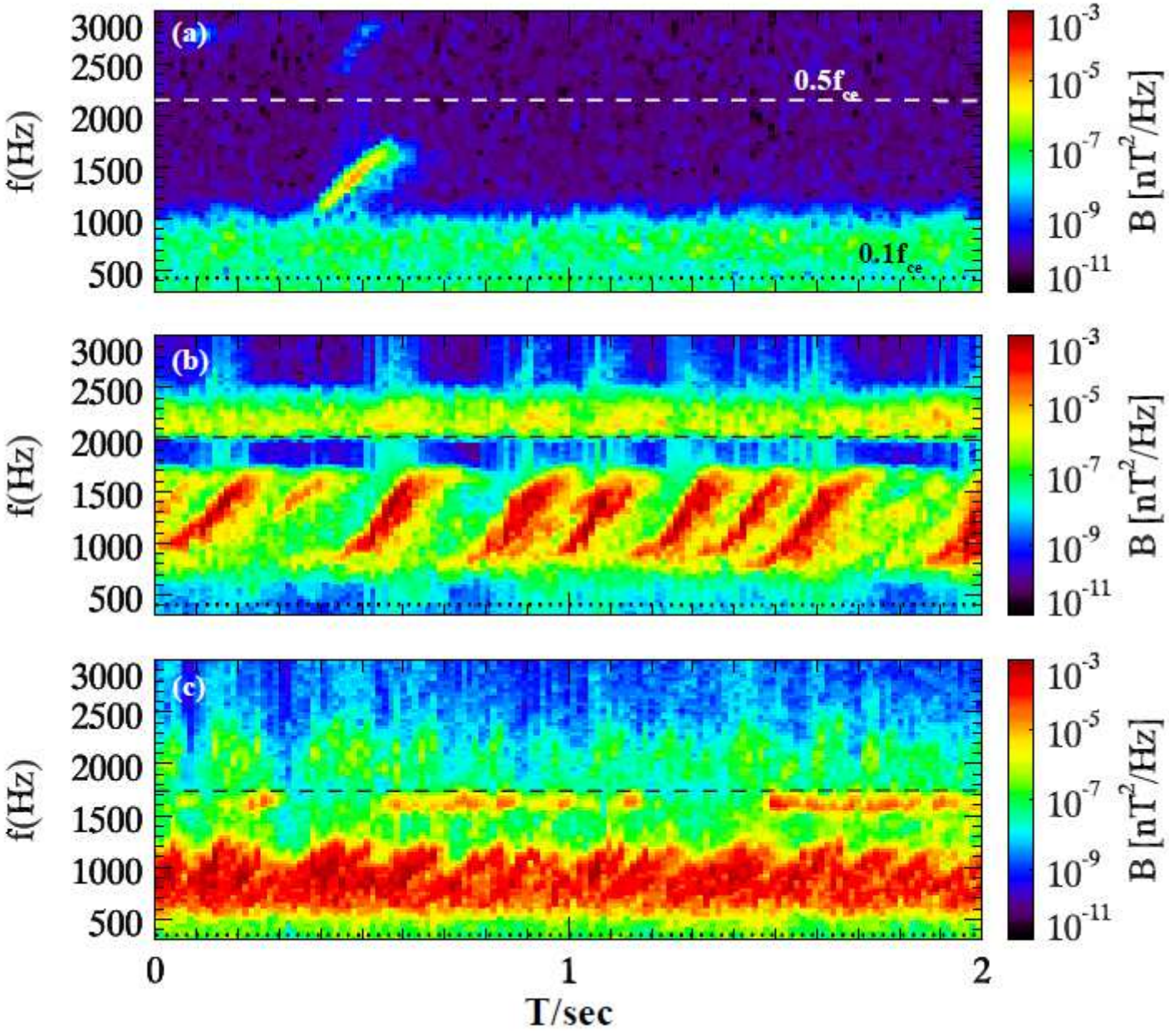

Figure 1

The spectrogram of magnetic power for three examples of chorus waves observed by the Van Allen Probes. All the chorus waves were detected by the Electric Magnetic Field Instrument Suite and Integrated Science (EMFISIS) on Van Allen Probe A. a The waves detected from 2014-04-30/19:33:29, in L-shell value=5.38, magnetic local time (MLT)=9.1hr, and magnetic latitude (MLAT)=-0.7o. There is only one discrete element. The background magnetic field is about 153.0nT, and the plasma density is about 9.1cm-3. The wave normal angle of the chorus waves is about 22.10, and the lowest frequency is about 1000Hz~0.23fce. b The wave detected from 2013-03-01/14:29:28.0, in L=5.06, MLT=2.7hr, and

MLAT=-0.9o. There is an ensemble of discrete and repetitive elements. The background magnetic field is about 144.6nT, and the plasma density is about 2.0cm-3. The wave normal angle of the chorus waves is about 11.10, and the lowest frequency is about 800Hz~0.20fce. c The waves detected from 2013-03-01/14:09:21.0, in L=5.31, MLT=2.4hr, and MLAT=-1.5o. The spectrogram looks like a continuous spectrum. The background magnetic field is about 124.7nT, and the plasma density is about 2.3cm-3. The wave normal angle of the chorus waves is about 21.40, and the lowest frequency is about 500Hz~0.14fce. In the figure, the dotted and dashed lines in black or white represent 0.1fce and 0.5fce, respectively. Here fce is the electron gyrofrequency at the equator.

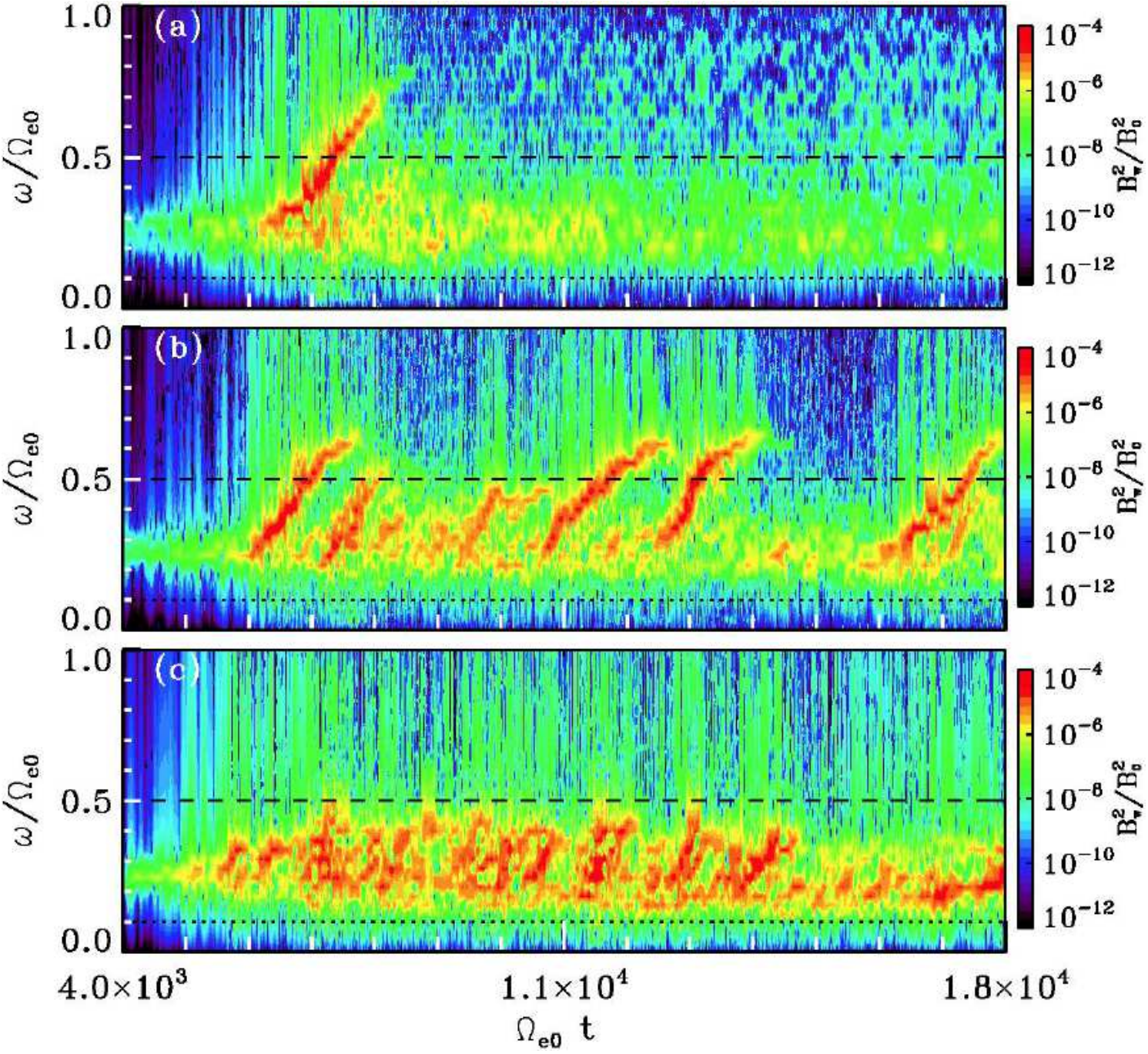

Figure 2

The spectrogram of magnetic power for chorus waves obtained at the latitude 150 from the simulations. a . b . c . Here, the dotted and dashed lines in black or white represent 0.1 and 0.5 , respectively, and is the electron gyrofrequency at the equator. The frequencies of these waves range from ~0.2 to ~0.75 .

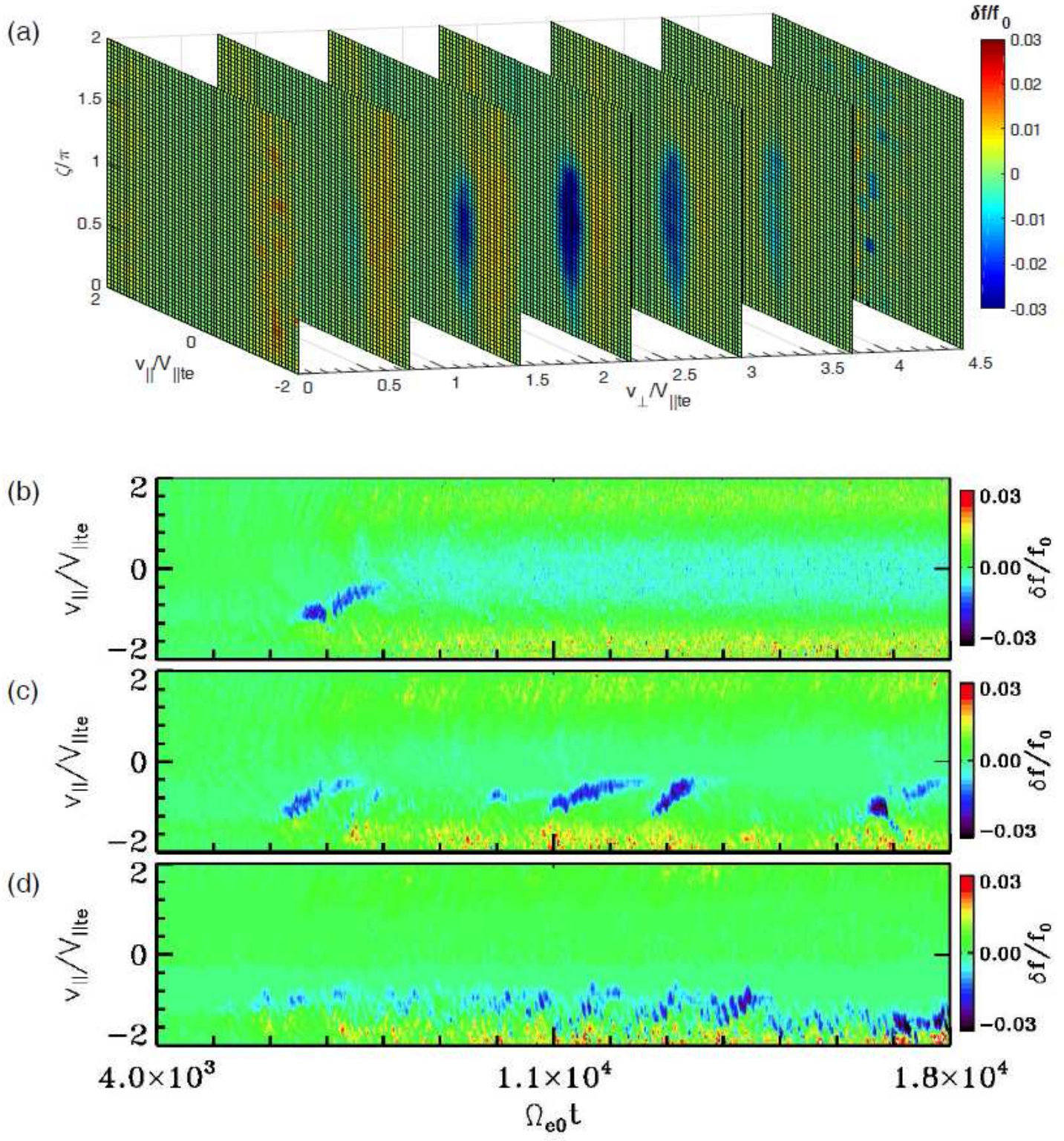

Figure 3

Electron holes associated with chorus waves obtained at the latitude 150 from the simulations. a Electron distributions at different values of for the selected hole at for the case with =2000. b-d The time evolution

of electron distributions at and =2.25 for the three cases, = , 2000, and 400, respectively.

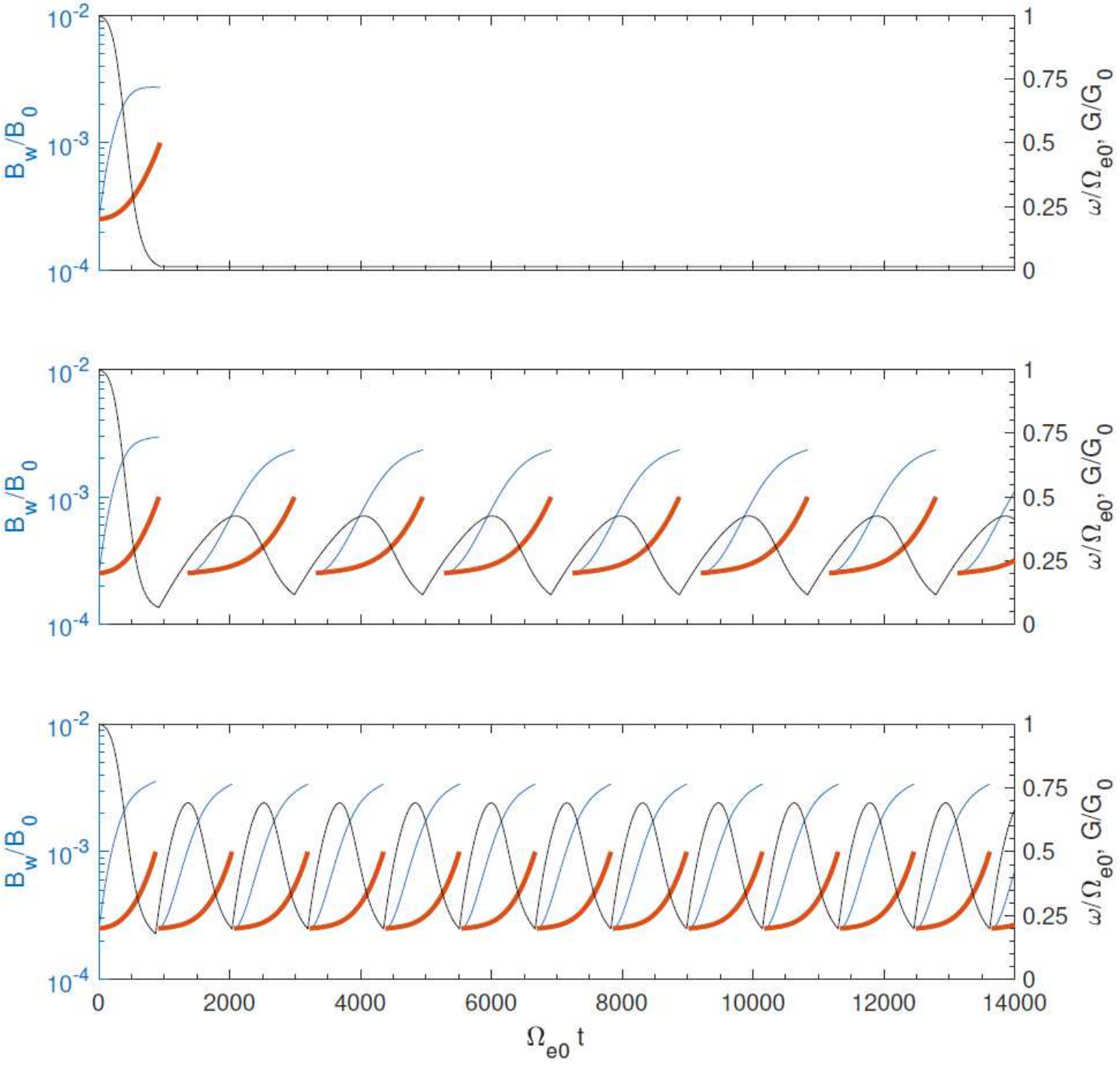

Figure 4

The time evolution for the amplitude ( ) and frequency ( ) of chorus waves, as well as the resonant distribution function ( ). a . b . c . The calculation is based on Eq. (1)-(3). The blue, red and black lines represent the amplitude ( ) , frequency ( ) and resonant distribution function ( ), respectively.

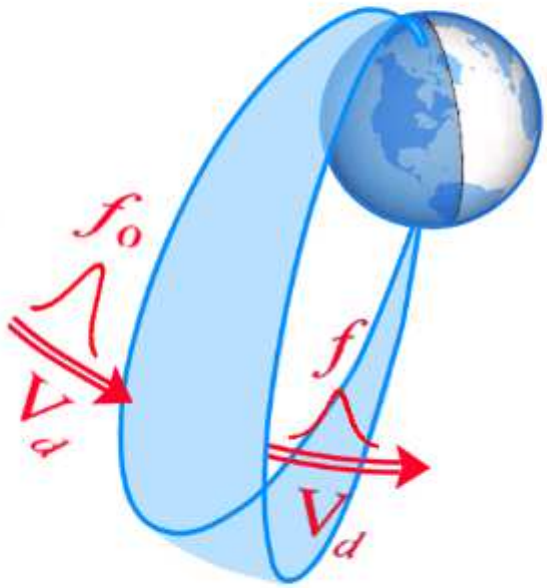

Figure 5

The schmetic diagram for the evolution of energetic electrons in a dipole magnetic field. Due to an azimuthal drift, energetic electrons with a distribution is injected into the simulation domain, while particles leaving the domain have a distribution . The blue-shaded region is the region of chorus wave excitation.